Computers and Electronics in Agriculture 119 (2015) 19–32

Contents lists available at ScienceDirect

Computers and Electronics in Agriculture

journal homepage: www.elsevier.com/locate/compag

Original papers

# Design of a low-cost Wireless Sensor Network with UAV mobile node for agricultural applications

Jose Polo *, Gemma Hornero, Coen Duijneveld, Alberto García, Oscar Casas

*Instrumentation, Sensor and Interfaces Group, Universitat Politècnica de Catalunya, BarcelonaTech, Spain*

ARTICLE INFO

*Article history:*
Received 13 March 2015
Received in revised form 15 September 2015
Accepted 26 September 2015
Available online 22 October 2015

*Keywords:*
WSN
UAV
Low-cost system
Agriculture

ABSTRACT

The aim of the present paper is to propose an agricultural environment monitoring server system utilizing a low-cost Wireless Sensor Network (WSN). Several sensor nodes are scattered in fields several kilometres in size, and we propose collection of the information stored in the nodes by a mobile node, or mule. To cover long distances in a short period of time, we use an unmanned aerial vehicle (UAV), which retrieves the data stored in the ground nodes. In addition, the UAV may be used to acquire additional information and to perform actions. Its elevated position allows observation of the field with a perspective that is useful for detecting changes affecting crops, such as pests, diseases, significant changes in soil moisture, drought or floods.



## 1. Introduction

Sensors are being introduced into almost every aspect of life. Agriculture is one such domain where sensors and their networks are successfully used to reap numerous benefits (Aqeel-ur-Rehman et al., 2014). The sensors can provide risk assessment information, for example, by alerting farmers at the onset of frost damage and providing better microclimate awareness. In precision agriculture, sensor networks enable an enhanced understanding of the changes in the crops to determine the optimum point for harvesting. They can improve the handling and management of water resources for irrigation, and they help to optimize fertilizer use and to increase crop performance (López Riquelme et al., 2009).

In a sensor network, the nodes must collect several measures of various parameters, such as temperature, humidity, and salinity, and they must transmit these measures, usually, to a central control. In field applications, due to the large distances, transmission must generally take place using a wireless network.

Wireless technologies have been under rapid development during recent years. The types of wireless technologies being developed range from simple IrDA, which uses infrared light for short-range, point-to-point communications, to wireless personal area networks (WPANs) for short-range, point-to-multipoint communications, such as Bluetooth and ZigBee, to mid-range, multi-hop wireless local area networks (WLANs), to long-distance cellular phone systems, such as GSM/GPRS and CDMA (Wang et al., 2006) networks.

The first application of a Wireless Sensor Network (WSN) in a greenhouse was reported in 2003. It was a monitoring and control system developed by means of Bluetooth (Liu and Ying, 2003). For applications where higher data rates are important, Bluetooth clearly has the advantage because it can support a wider range of traffic types than ZigBee. However, ZigBee is designed for devices with low power consumption and has a range of approximately 10 m to 100 m (ZigBee Specification FAQ).

Most crop fields are extensive, with a size of up to several kilometres. In this type of field, the distance between nodes needed to cover the whole area can be large. Hence, it is necessary to use radio extenders, to use other wireless protocols or to increase the power of transmission, thereby increasing the energy consumption (Ruiz-Garcia et al., 2009). To avoid this increase in the energy consumption, the nodes can be located sufficiently close to one other, which requires an increase in the number of nodes.

We propose the use of a sensor network for extensive fields where the nodes are not capable of communicating amongst themselves directly, and a mobile node is used to collect the data from the static nodes. The mobile node moves from one node to another node. If the mobile node is installed in an aerial vehicle, it can access any position, no matter its location or distance; its travel speed is sufficient to reach distant points in short periods of time, and it is a low cost system.

For monitoring plants in fields, in addition to the variables taken by the ground nodes, it is very helpful to have other

* Corresponding author.
*E-mail address:* jose.polo@upc.edu (J. Polo).

http://dx.doi.org/10.1016/j.compag.2015.09.024
0168-1699/

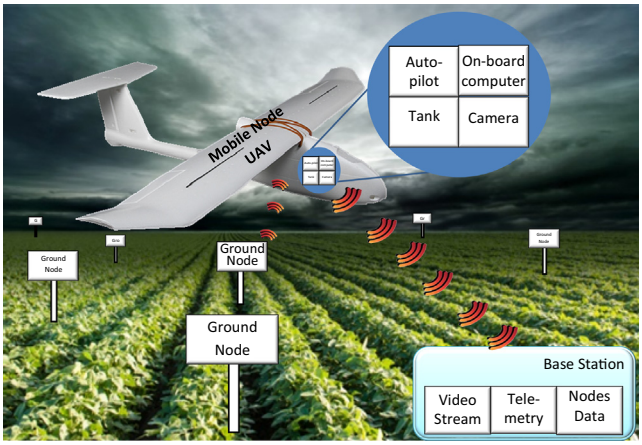


**Fig. 1.** System architecture.

measures affecting large areas of the field. Aerial images can be used to detect water accumulation on plant surfaces or on the ground. The appearance of crops or the colour of plants often changes when they suffer from a disease or a pest. These images can be obtained using satellites or manned aircraft, but they are expensive. Alternatively, a camera carried by an aerial vehicle can acquire those images. Using infrared imaging, it is possible to measure moisture on crops (Stafford et al., 1989) or soil (Ayalew and Ward, 2000; Hassan-Esfahani et al., 2014; Hea et al., 2007; Yin et al., 2013).

Another important point to highlight is that an aerial vehicle can be used to act on the environment, which is an important advantage. For example, if a disease or pest is detected, pesticides or insecticides can be used to fight them. The vehicle is able to transport these substances and release them at a particular point when necessary.

Finally, to improve the vehicle's manageability and usability, it would be very helpful if it could fly autonomously or could be guided manually.

Therefore, the aim of this work is to create a network of sensors that can be applied in agricultural operations with extensive fields. Using several low-cost sensor nodes scattered throughout the field and a low-cost mobile sensor node, not only can the data from the ground nodes be recovered but global measures of the crops can also be obtained from the sensors carried by the UAV, including video measures (using a image sensor), and the UAV can act if necessary. The mobile node sends all the collected information to a base station wirelessly. Fig. 1 shows architecture of the developed system.

## 2. Materials and methods

When fields are very extensive, the nodes of the network are too far apart to communicate amongst themselves. A mobile node, or mule, is carried by the aerial vehicle, and to include the above features, it must meet several requirements:

- The distance to overcome can be several kilometres. To achieve good autonomy, a low consumption system is necessary. The vehicle must be able to cover distances of up to 10 km or to operate in fields of approximately 100 ha.
- The vehicle will fly above the nodes at a certain distance. The communication range must be sufficient to enable the mobile node to communicate with the sensor nodes dispersed on the ground and to collect the data stored in them.
- To detect situations of disease or pests in crops, the images should be of high quality. The vehicle must send a live video stream with sufficiently high quality to show changes in crops and store the video for later processing.
- If a disease or pest is detected, the application of a substance to counteract them can be useful. The vehicle must be able to transport these substances and launch them in the required positions.
- To obtain a system that is not too expensive, the total cost must be kept as low as possible, within a budget of $1000.

The candidate vehicle that has the desired features and meets the requirements is a UAV. During the past several years, these devices have become more and more popular, and their applications are growing continuously.

A UAV is defined as an aircraft that does not carry a human operator, is operated remotely using various levels of automated functions, and is normally recoverable. There are different types of UAVs, and they can be classified in different ways, including by who is operating it, the flight type, the size, the payload, and the level of automation. One way to classify UAVs is by the flight type, which is primarily either rotorcraft or fixed wing but is occasionally another, such as balloon, kite, or ducted fan technology. Rotorcrafts (Fig. 2 left), which usually have two to eight rotor propellers, have the advantages of hovering to collect imagery and taking off and landing vertically (VTOL or vertical take-off and landing); however, they deplete batteries quickly because much of their energy is dedicated to vertical lift, and thus they are limited in time aloft to typically less than 30 min. Japan, for example, is a pioneer in the application of rotorcraft UAVs to agriculture. For 30 years, environmental parameters have been monitored by remotely controlled helicopters, called "aero-robots" (Lee, 2014).

Fixed wing UAVs (Fig. 2 right) can fly longer distances for longer times, usually 45 min to several hours, making them more effective for collecting imagery over a wide area, but they need space for takeoff and landing and cannot hover (HTOL or horizontal take-off and landing). They are capable of moving at higher speeds carrying heavier payloads with lower energy consumption, and they have great autonomy, but they cannot execute VTOL manoeuvres or high-precision movements.

This type of vehicle is currently used for several applications such as for agriculture, the film and broadcast industries, pollution measurements, surveillance, communications relays and so on (Bento, 2008; Benett, 2014).

Considering the amount of equipment that needs to be carried and the energy requirements to extend the range to the required distance, a good option for our agriculture network is to use a fixed-wing architecture.

The fixed-wing UAVs have swept back wings, and the tip aerofoils have a greatly reduced incidence compared with the aerofoils of the inner wing. This ensures that as the aircraft nose rises, the wing's centre of lift moves towards the rear, thus returning the aircraft to its original attitude. The performance of these aircraft suffers because of the reduced effective tail-arm in both the pitch and yaw axes, although the rearward sweep of the wing does add to the directional stability (Austin, 2010).

The developed vehicle is divided into two main parts: (1) the plane itself, which is composed of several subsystems that are needed to fly properly, and (2) the payload, which consists of several subsystems to achieve the desired features.

The plane architecture contains the following subsystems:

- Airframe: it is the body of the whole system. It carries all of the other subsystems and allows the plane to fly by generating lift.

**Fig. 2.** UAV types: rotorcraft, left, fixed-wing, right.

- Autopilot: it is in charge of controlling and navigating the aeroplane.
- Motor and propeller: they give energy to the aeroplane to generate lift and fly.
- Power supply: It powers the entire system.

Fig. 3 shows the relationship amongst the subsystems of the plane architecture.

The airframe carries the payload, and the power supply provides energy to all of the plane systems, as in Fig. 4. The payload architecture contains followings subsystems:

- Mobile sensor node: it collects the data from the ground sensor network.
- On-board computer: it is used to transmit and store real time video and telemetry over the Internet, as well as to gather data from sensors.
- Camera: the camera is used to capture video in flight; this video is then processed by the on-board computer.
- Small tank containing the product to be scattered.

Furthermore, in addition to the aerial vehicle, there is a ground control station consisting of a ground computer subsystem that receives the telemetry data, the video stream and the network sensor data from the plane and allows the operator to know, at any moment, the status of the plane and its contents.

### 2.1. The plane

The main plane component is the airframe, which is the structure that carries all of the other subsystems. The airframe must meet several requirements: (1) the total weight of the plane must be 5 kg; (2) it must have a load bay that is large enough to transport all of the components and that is easily detachable; (3) in the case of an accident, the plane must be strong enough to survive without fatal damage; and (4) it must cost as little as possible.

Several types of materials are used to build aircraft models, such as fibreglass, wood and foams such as EPP (expanded polypropylene) or EPO (expanded polyolefin). Fibreglass and wood are light materials commonly used for manufacturing RC (Radio Controlled) aeroplanes, but they have poor crash resistance. Thus, a foam aeroplane is chosen. In particular, the airframe selected is the Skywalker 1900 mm wingspan platform; see Fig. 5. Its main dimensions are as follows: wingspan 1900 mm, length 1180 mm, wing area 35.5 dm$^2$, cabin size 120 mm × 370 mm × 72 mm, and flying weight 1300 g to 1800 g.

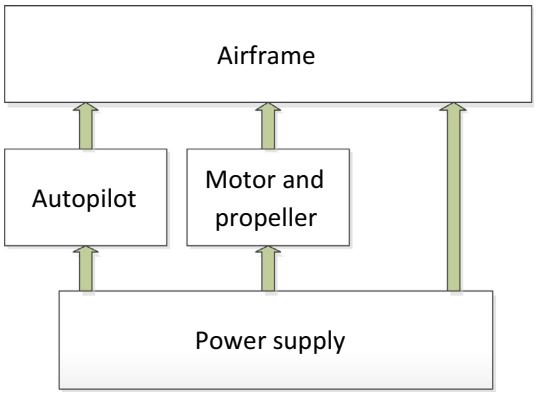


**Fig. 3.** Plane architecture and the relationship between the subsystems.

The propeller is a very important part of the aeroplane because it converts the rotational power transmitted from the motor into thrust, and this thrust is used to accelerate the plane. In RC aircraft, propellers are classified by two lengths: the first one refers to the diameter and the second to the pitch length. Fig. 6 shows the length and the pitch of a propeller. Both are normally given in inches. The first parameter is easily understandable because it is simply the length of the prop from tip to tip. The pitch length, which is usually referred to simply as the pitch, is similar to that of a common screw. If the propeller were turned through the air without slipping, the distance it would travel in each revolution is called the pitch length (Phillips, 2010). It is important to choose the correct propeller for the motor and airframe.

In the following calculations, the propeller's forward motion will be considered to be completely perpendicular to the axis of rotation, that is, no component of the forward airspeed is in the plane of rotation.

The total thrust developed by a propeller can be calculated with the following equation:

$$T = \frac{k\rho\omega^2}{2}\int_{r_k}^{r_t} r^2 c_b \frac{\cos^2\varepsilon_i}{\cos^2\varepsilon_\infty}\left[\tilde{C}_L\cos(\varepsilon_\infty+\varepsilon_i) - \tilde{C}_D\sin(\varepsilon_\infty+\varepsilon_i)\right]\mathrm{d}r$$

where $\varepsilon_i$ is the induced angle and can be numerically determined using the following equation:

$$\frac{kc_b}{16r}\tilde{C}_L - \cos^{-1}\left[\exp\left(-\frac{k\left(1-\frac{2r}{d_p}\right)}{2\sin\beta_t}\right)\right]\tan\varepsilon_i\sin(\varepsilon_\infty+\varepsilon_i) = 0$$

where $k$ is the number of propeller blades, $r$ is the air density, $\omega$ is the rotational speed of the propeller, $r_t$ is the tip radius, $r_h$ is the hub radius, $c_b$ is the local section chord length, $e_i$ is the induced angle, $e_\infty$ is the downwash angle that results from the propeller's forward motion, $\tilde{C}_L$ is the local section lift coefficient, $\tilde{C}_D$ is the local two-dimensional section drag coefficient, $d_p$ is the propeller diameter, and $b_t$ is the aerodynamic pitch angle at the propeller blade tip.

The thrust can be computed if the parameters are known. The pitch length can be obtained from the pitch angle $b$ with the following relation.

$$\lambda(r) = 2\pi r\tan\beta$$

The total torque required to turn the propeller is:

$$l = \frac{k\rho\omega^2}{2}\int_{r_k}^{r_0} r^3 c_b \frac{\cos^2\varepsilon_i}{\cos^2\varepsilon_\infty}\left[\overline{C}_D\cos(\varepsilon_\infty+\varepsilon_i) + \overline{C}_L\sin(\varepsilon_\infty+\varepsilon_i)\right]\mathrm{d}r$$

If the torque is multiplied by the angular velocity, then the brake power $P_b$ is obtained:

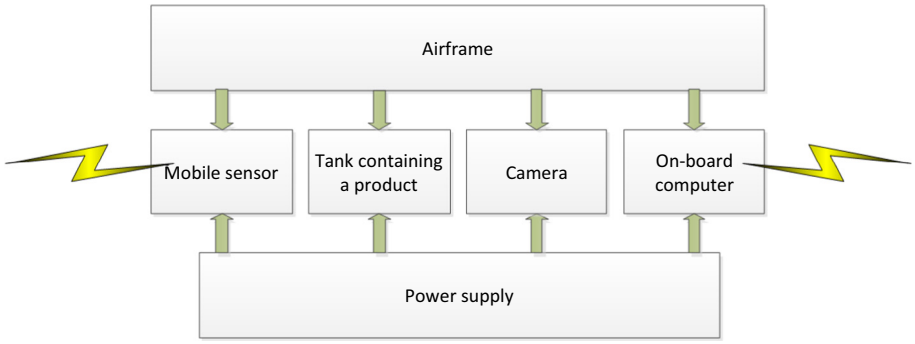


**Fig. 4.** The airframe carries the payload: mobile sensor node, tank, camera and computer. The power supply provides energy to the payload.

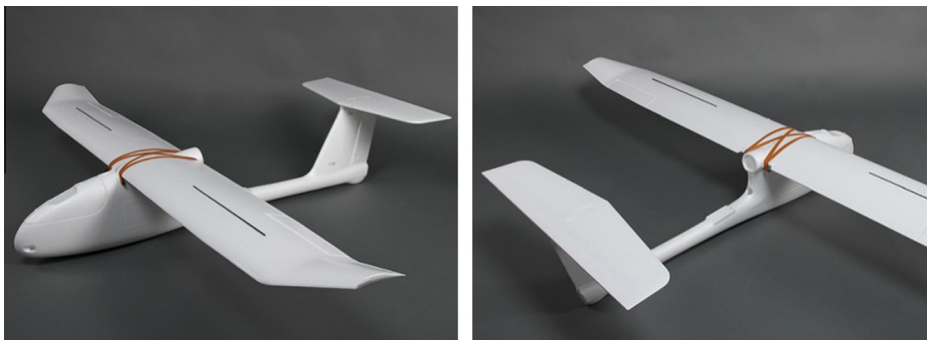

**Fig. 5.** Skywalker 1900 mm wingspan platform.

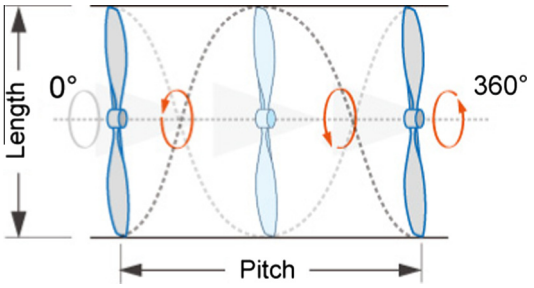


**Fig. 6.** Length and pitch of a propeller.

$$P_b = l\omega$$

Keep in mind that most of the complexity regarding these equations resides in the lift and drag coefficients, which are somewhat difficult to calculate. Using the experimental measures of N.A.C.A report No. 502 (Silverstein, 1934), which contains information regarding the Clark Y airfoil, which is similar to our airframe, we can estimated the lift (CL) and drag (CD) coefficients as:

$$C_L = 4.01\alpha_b$$

$$C_D = 0.687\alpha_b^2 + 0.337\alpha_b + 0.054$$

where $\alpha_b$ is aerodynamic angle of attack of our airframe. With this model, several calculations have been made for a forward speed of 35 knots (kt) (as it is considered the maximum achievable cruise speed) and several propeller sizes. The results of these calculations will be the powers required to turn the motor, and they are shown in Table 1.

From the results in Table 1, it is seen that the power needed to turn the propeller remains approximately constant for the same pitch, but the required rpm value decreases as the diameter increases. It is better to achieve the desired thrust with lower rpm because the propeller will be subject to lower rotational forces. For lower rpm, a larger diameter is needed. The Skywalker has a propeller size limit due to its structure. The maximum propeller size is 9 in. For a longer size, it hits the tail; see Fig. 7. Table 1 shows the results for a 9, 8 and 7-in. propellers with different pitch lengths. Note that as the pitch length decreases, more rpm are needed to provide the same thrust, and the higher rpm value results in increased drag that the motor has to overcome, and thus more power is needed. Finally, we selected an APC 9 × 4.5; therefore, the selected pitch for the propeller was 4.5 in. The selected propeller was NTM Prop Drive Series 35–30 A 1400 kV.

The power is supplied by a rechargeable battery, of which there are different types: Nickel–Cadmium (NiCd), Nickel-Metal Hydride (NiMH), Lithium-ion (Li-ion) and Lithium-Polymer (LiPo). The last of these, LiPo batteries, are chosen mainly due to their high specific energy, low weight and the fact that they can supply higher discharge rates. Special safety measurements have been followed to ensure safe use. Base on the motor requirements, a 3S battery has been chosen. The LiPo cells have a nominal voltage of 3.7 V; thus, three cells have a nominal voltage of 11.1 V. The necessary capacity of the battery is determined by computing the energy consumption of the system during nominal operation. The capability of flying distances of up to 10 km was an initial project specification, and at the cruise speed of 35 kt (knots), the time to fly 10 km is 9.26 min. Using this time and the results obtained from the power requirements of the motor, the capacity of the battery can be determined. To maintain level flight at a cruise speed of 35 kt, the motor must provide 269 W; see Table 1. Therefore, the battery must provide a current of 24.3 A, considering that its voltage is 11.1 V. This current requirement multiplied by the 9.26 min necessary to travel 10 km results in a required battery capacity of approximately 3800 mA h. In the design, a Turnigy nano-tech 8400 mA h 3S 40–80 C Lipo Pack (Slash VXL/Slash 4 × 4) battery

**Table 1**
Results of calculations for several propellers sizes. The values of the size column are the length × the pitch of the propeller. The selected propeller is highlighted. The results have been created using the previous equations.

| Size | RPM | Power (W) | Size | RPM | Power (W) | Size | RPM | Power (W) |
|---|---|---|---|---|---|---|---|---|
| 9 × 3 | 13,550 | 354 | 8 × 3 | 15,070 | 332 | 7 × 3 | 17,150 | 320 |
| 9 × 4 | 11,750 | 290 | 8 × 4 | 13,100 | 281 | 7 × 4 | 14,800 | 270 |
| **9 × 4.5** | **11,050** | **269** | 8 × 4.5 | 12,300 | 261 | 7 × 4.5 | 13,950 | 257 |
| 9 × 5 | 10,450 | 253 | 8 × 5 | 11,620 | 247 | 7 × 5 | 13,200 | 245 |
| 9 × 6 | 9480 | 230 | 8 × 6 | 10,600 | 231 | 7 × 6 | 12,500 | 232 |
| 9 × 7 | 8750 | 217 | 8 × 7 | 9800 | 220 | 7 × 7 | 11,150 | 223 |
| 9 × 8 | 8150 | 208 | 8 × 8 | 9100 | 209 | 7 × 8 | 10,450 | 217 |
| 9 × 9 | 7700 | 204 | 8 × 9 | 8600 | 205 | 7 × 9 | 9900 | 214 |
| 9 × 10 | 7300 | 200 | 8 × 10 | 8170 | 201 | 7 × 10 | 9450 | 212 |

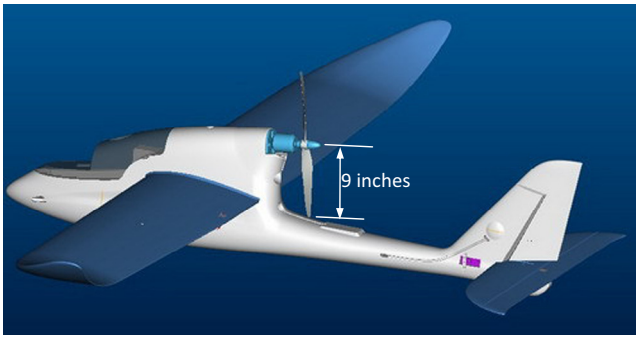


**Fig. 7.** Distance between the propeller and tail.

was used for powering the propeller system. This battery provides approximately 25 min of autonomous operation, and the range is approximately 27 km.

The autopilot is the most important electronic component carried by the plane. It is the element responsible for navigating the plane and guides the plane without assistance from human operators (Chao et al., 2007). It can be programmed to follow a track. The autopilot needs to communicate with the ground station for control mode switching, receive broadcasts from GPS satellites for position updates and send out control inputs to the servo motors on the plane (Chao et al., 2007). The controlling is usually performed by a processor.

A wide variety of autopilots is available. The first selection was based on the price. There are autopilots ranging in price from approximately $200 to $1000 (3DRobotics, Cloud Cap Technology, or OpenPilot) to approximately $10,000 (Lockheed Martin or MicroPilot). To fit within the budget, the cost of the preselected autopilots is several hundreds of dollars: from $200 to $500. 3DRobotics presents solutions for UAVs and has the philosophy of providing free hardware.

Four autopilots were selected, and their technical specifications are as follows:

(a) PX4 FMU (3DRobotics). It has a Cortex-M4 168 MHz processor, with a flash memory of 1024 KiB and RAM of 192 KiB. The reference gyro and accelerometer are integrated in the MPU6000, and the maximum ranges of these elements are to ±2000°/s and ±16 g, respectively. The reference magnetometer is the HMC5883L. To measure air velocity, a reference barometer MS5611 is used, which has an altitude resolution up to 10 cm and works at a voltage of 1.8–3.6 V (Measurements Specialities, 2012). This autopilot has eight outputs for actuators, dimensions of 50 mm × 36 mm × 6 mm, a weight of 9.62 g and a price of $390.

(b) 3DR Pixhawk (3DRobotics). It features a 32-bit processor ARM Cortex M4 core at 168 MHz, 2 MiB flash memory, and 256 KiB RAM. The accelerometer and magnetometer come in a single component called the ST Micro LSM303D, and the maximum mean these sensors can handle are ±16 g and ±12 g, respectively. These elements respond up to 400 kHz and work with a voltage of 2.16–3.6 V (ST, 2013). The gyro reference is the T Micro L3GD20. As in the case of the PX4 FMU autopilot, an MS5611 reference barometer is used to measure the air velocity. The 3DR Pixhawk has 14 output ports for servomotors, the dimensions are 81 mm × 50 mm × 15 mm, it weighs 28 g and is priced at $380.

(c) APM 2.6 set (3DRobotics). The autopilot has an ATmega2560 processor, which is an Arduino component that can be reprogrammed by the user and operates at 16 MHz, and it has 2564 KiB of flash memory. The reference gyro and accelerometer with this autopilot is the MPU6000, as in the case of the PX4 FMU. This autopilot can accommodate eight outputs and eight inputs, has dimensions of 70 mm × 45 mm × 15 mm, weighs 33 g and is priced at $240.

(d) CopterControl (OpenPilot). The CopterControl & CC3D boards are an all-in-one stabilization hardware platform that runs the OpenPilot firmware. It can fly any airframe from a fixed-wing to an octocopter and is configured and monitored using the OpenPilot Ground Control Station (GCS) software. The CopterControl hardware has the following features: an STM32 32-bit microcontroller running at 90 MIPs with 128 KiB Flash and 20 KiB RAM, 3-axis high-performance MEMs gyros and a 3-axis high-performance MEMs accelerometer. Its 4-layer PCB has dimensions of 36 mm × 36 mm and has USB support with no drivers required – a truly plug and play device – and a 4 Mibits on-board EEPROM for configuration storage. It also offers a port that provides either I2 C connectivity or a second serial port. Its price is approximately $200.

Although the APM2.6 autopilot has been selected as the best choice because of its vast usage community and its maturity, the 3DR Pixhawk could be a good alternative because it has better performance than the APM2.6, it is being included in an increasing number of designs, more groups are working with it, and the experience level continues to grow.

The autopilot has been configured using a series of parameters to control the autopilot's behaviour. A list of all of the parameters is described at http://plane.ardupilot.com/wiki/arduplane-parameters/. These parameters define the flight controller, i.e., they define the PIDs that control the roll, yaw, and pitch, and it is very important that they be configured correctly. The tuning of the PID parameters was performed in flight to test the aeroplane's behaviour (first tests), but a configuration file from another DYDrones user named Ryan was created for our 1900 mm wingspan platform (DIYDrones. Skywalker parameter file. http://diydrones.com/forum/topics/skywalker-param-file-wanted).

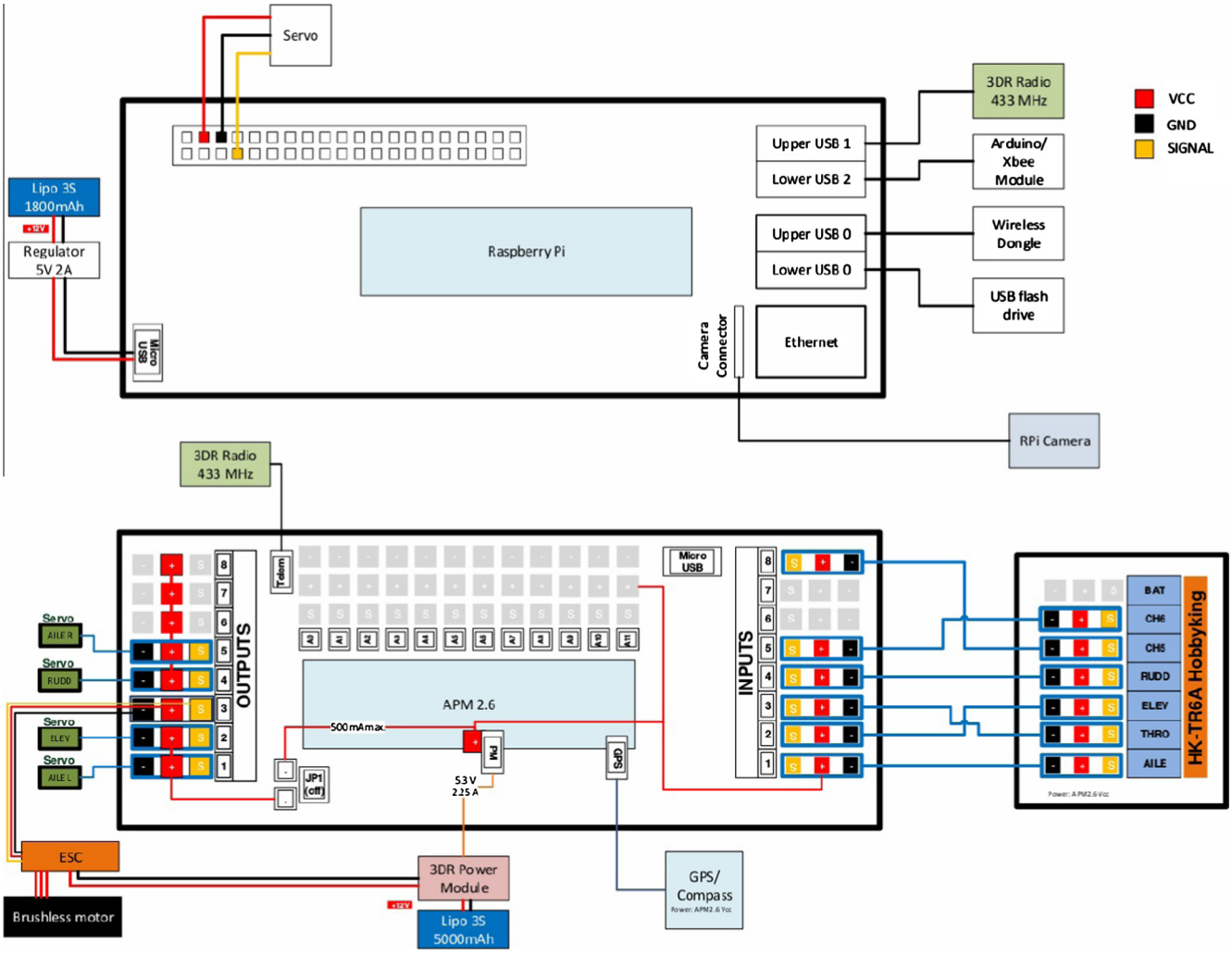


**Fig. 8.** Connection architecture.

*2.2. The payload*

The payload comprises the subsystems that the plane carries to achieve the desired functionality. The vehicle must perform six main tasks:

1. receive and store information fetched from ground sensors,
2. transmit the data obtained from the nodes,
3. transmit the aeroplane's telemetry messages,
4. receive and transmit orders and instructions to the autopilot,
5. stream a first person view low-latency video and
6. perform the actions in response, when required.

The system sends and receives several types of data streams. This prototype check if it is possible to transmit properly all streams, but a real application would transmit only necessary streams.

Fig. 8 shows the connection architecture of the components of the system. The largest modules are the autopilot and the on-board computer.

Most of these tasks are performed by the on-board computer. This computer must meet several requirements: low price and weight, Internet connectivity, real-time data handling, transmission and storage capability, capacity to stream a video to the Internet, capacity to deal with several external devices.

During recent years, there has been broad development of systems that fit those requirements. Several boards have been studied to select a candidate: Banana Pi, BeagleBone, HummingBoard, MinnowBoard, and Raspberry Pi. Each is a computer in a board approximately the size of a credit card. The CPU clock runs at approximately 1 GHz. They have between 0.5 GiB and 2 GiB of RAM. They have several communications connectors: LAN, USB, HDMI or composite video.

To take a decision, we have compared several characteristics: the CPU, RAM, connectivity, community and costs. Fig. 9 shows several benchmark comparisons amongst the boards. From those results, a radar plot has been prepared and is shown in the lower right of Fig. 9. We have opted to use this benchmark plot. The best board is the one that covers the largest area. The Raspberry Pi covers almost twice the area of the board covering the next highest area, the MinnowBoard. The Raspberry Pi's strengths are the low cost, the vast number of users and the resulting huge variety of applications and accessories for the board, and the connectivity. On the other hand, its worst faults are the CPU and the RAM; however, for our application, the capacity is sufficient to perform properly.

The choice is thus the Raspberry Pi. This board can be defined as a low-cost, low-weight, low-size computer capable of running a complete Linux distribution.

The plane carries the mobile node and flies over the ground nodes to harvest the data they have measured and stored in their

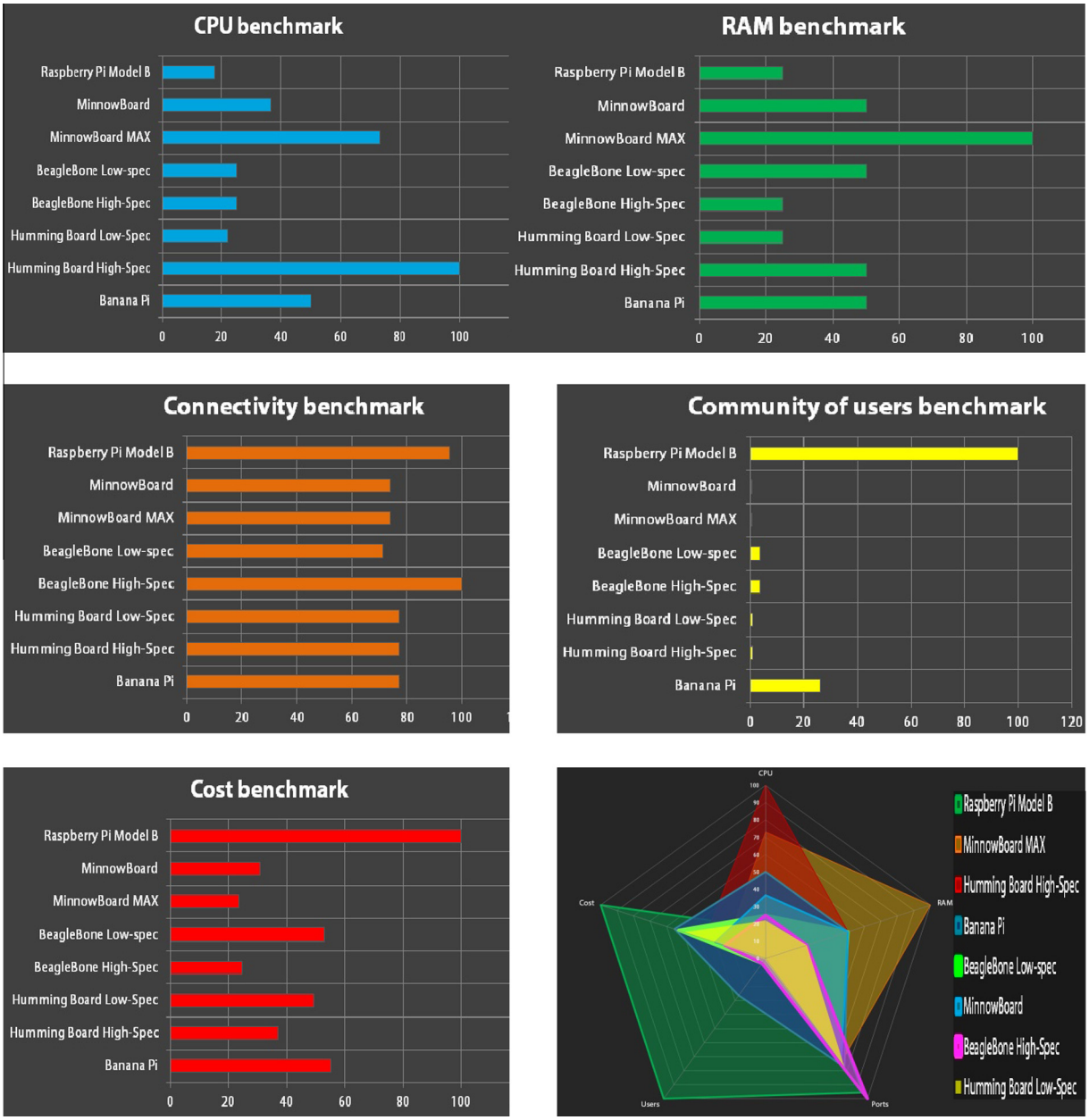


**Fig. 9.** Benchmark comparison of several characteristics amongst several computers. These graphs have been created using the specifications and information obtained from the manufacturers of the computers.

memories. The on-board computer stores and transmits the collected data.

In this application, Arduino is the choice for the network nodes because there are thousands of compatible devices and it is a low cost platform. The on-board mobile Arduino node, connected to the Raspberry Pi, acquires the data collected by the ground nodes. Then, the on-board mobile node transfers those data to the Raspberry Pi, which transmits the data using its Internet connection.

The communication between the on-board node and a ground node is performed by the ZigBee wireless protocol. This protocol permits data rates ranging from 20 to 250 kbps, which is valid for this application. It is oriented towards low power consumption, it uses IEEE 802.15.4, and it is low cost (ZigBee Features). To use ZigBee with the Arduino, a Digi XBee module is employed. This module has a range of 90 m (outdoor) and a data rate of 250 kbps. It operates at 2.4 GHz and can address 65,000 addresses. Its power consumption is a maximum of 50 mA (when receiving) and a minimum of less than 10 μA when in the sleep mode, and it can operate from −40 °C to 85 °C (XBee).

The ground nodes are equipped with a temperature and humidity sensor: a Rotronic HygroClip HC2-S3. Its main features are:

- Humidity measuring range: 0–100 %RH.
- Temperature limits: −50 to 100 °C.
- Accuracy: ±0.8 %RH, ±0.1 K at 10–30 °C.
- Diameter: 15 mm.
- Length: 85 mm.

Fig. 10 shows this sensor (right) and a node (left) used to collect and send its data. The analogue data from the sensor is digitalized by the microcontroller of the Arduino, which uses an ATmega328. Its AD converters use 10 bits, and they have an error of ±2 LSB. The error measurements, accounting for the sensor and AD converters errors, are:

- Humidity: ±1 %RH.
- Temperature: ±0.1 K.

The node makes a measurement every ten minutes and stores it in its memory. The mobile node collects the data once per day.

The vehicle has to transmit different types of data to the control point or base station, and for this purpose, a wireless point-to-point connection can be used. The vehicle carries a transmitter and the base station uses a receiver. This solution has a maximum range of actuation of a few kilometres, but to extend the range, the wireless telephone network was chosen. This option allows operation regardless of the range or location. It depends only on the mobile telephone coverage. For good transmission speed, at least, a 3G connection must be used. In our country 3G connection is a good option because the coverage covers more than 97% of the population, and there are cheap flat rates. This network permits a wide range with a sufficient throughput and allows the on-board autopilot to communicate with the ground computer to transmit orders and telemetry messages using the Internet.

The plane carries an image sensor: a camera to transmit a first person view video. Usually, this functionality is achieved using a video transmitter/receiver set; however, these sets are expensive, heavy, and have a rather limited range and offer only a low image quality, which are the main drawbacks, and they have a low-delay signal, which is their greatest advantage. Furthermore, these systems have incompatibility with the allocated frequency spectrum, depending on the country. This fact could cause signal loss due to interference and may also be illegal. Our solution is to use the Raspberry Pi. A webcam can be directly connected to stream video through the Internet. Its main advantages are low cost, low weight and that is a fully legal system, but the main drawback may be the latency of the signal.

There is huge number of compatible cameras to use with Raspberry Pi (RPi USB Webcams). Several parameters were studied for selecting a camera: the resolution, the image quality, the weight and the price. The Raspberry Pi's camera module was selected. This module is designed to be used only with the Raspberry Pi. It has a resolution of 5 MP, is capable to take video at a resolution up to 1920 × 1080 pixels (Full HD) at 30 FPS and weighs 3 g.

In agriculture is usual to use infrared images for remote sensing of moisture, detection of fungal infection and other crop assessments (Hunt et al., 2014; Liang et al., 2015; Suchata et al., 2015; Weyrich et al., 2013). Therefore, the selected camera is sensitive to infrared (IR) light. Actually, it is a normal camera (current cameras are sensitive to visible and IR lights) without IR optical filter. Thus, the captured images are a bit odd. Fig. 11 shows this effect. The camera acquires night-vision videos when an area is illuminated with infrared light, which is invisible to humans.

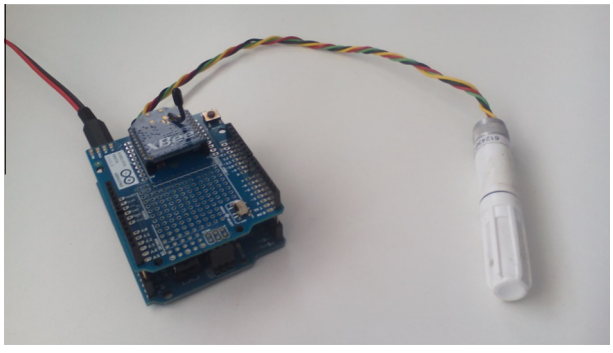

**Fig. 10.** Node (left) and sensor (right). The node is composed of an Arduino, a shield and an XBee module. The sensor, a Rotronic HygroClip HC2-S, can measure temperature and humidity.

If a disease or a pest is detected, the operator can scatter a product to fight them. While a plane is not a good vehicle to spray a substance, a rotorcraft is a better option, this functionality was added to test its performance. The plane transports a tank containing, for instance, an insecticide, herbicide, fertilizer, etc. This tank can be opened by the operator at any time, when necessary. The tank is controlled by the Raspberry Pi, which receives orders from the operator. The tank cap is moved using a servomotor. When opened, the contents are released.

The total cost of the system was approximately $900. Table 2 shows the different components and their prices. The total cost is low enough to introduce the sensor network with a mobile node in any application with a large network. It can be applied to supervise agricultural applications in which the large dimensions of the field make it difficult to use a traditional sensor network.

### 2.3. Plane control

The plane receives and sends several types of information: it fetches data from ground sensors, dispatches the video stream, transmits plane telemetry, gathers orders for the autopilot or commands for controlling the flight and receives orders to act after detection of a pest or a disease. Fig. 12 shows the communication amongst these modules.

The nodes scattered around the field collect environmental data. They store these data until the mobile node is carried near enough by the plane, and then the ground node sends the data to the on-board node using the ZigBee protocol. This protocol uses the ISM band for communicating (Higuera and Polo, 2011). The usual frequency is 2.4 GHz, but some other wireless protocols use this frequency, for example, WiFi (Radio Regulations). The fact that different protocols can use the same frequency can cause a problem. Another possibility is to use another frequency. An alternative is 5.8 GHz (Radio Regulations), but this frequency is shared, too; furthermore, its range is smaller. Another legal lower band where data links can be found is at 433 MHz, which is where the telemetry set works, and, therefore, it is not a valid alternative. Thus, the selected frequency is 2.4 GHz. Fields are usually located in rural areas, where few transmissions are expected at that frequency. Therefore, the use of the 2.4 GHz band will probably not be problematic.

The system has several wireless devices that transmit in the ISM band. These devices use various interference management techniques to minimise the interference due to use of the same frequency band. These are the frequency-hopping spread spectrum (FHSS) and direct-sequence spread spectrum (DSSS) techniques (Chiasserini and Rao, 2003). Furthermore, the transmission protocols are designed to detect cases of data lost because of mutual interference, and, if necessary, the devices retransmit the data until it is received correctly.

To save energy, the ground nodes are sleeping most of the time, and they wake up periodically to perform measurements. The on-board node wakes up the ground nodes to fetch the measured data. To perform this operation, the on-board node sends an encoded radio signal, using a small transmitter that is heard by the ground nodes. They are completely asleep, except for a small receiver that is listening for this signal. This small receiver has a consumption of 75 μA (Abacom ARX-433-ULC).

The plane carries a image sensor to transmit a first person view video for searching for a disease or a pest. The camera selection was discussed in the previous section. The camera is attached to the Raspberry Pi by its CSI port. The raspberry Pi can capture video or still images into its SD memory card or can send them using the Internet 3G connection. The second option is adequate for searching for a disease or pest. Although the camera can obtain Full HD videos, it is necessary to maintain the Raspberry resource usage

**Fig. 11.** Images captured using a normal camera (left) and an infrared camera (right).

**Table 2**
Components, vendors, quantities and costs. The total value of the entire system is $946.76.

| Component | Cost per unit ($) | Units | Total cost ($) |
|---|---|---|---|
| APM 2.6 Set + Assembled + Power Module | 143.99 | 1 | 143.99 |
| 3DR Radio Set (frequency: 433 MHz) | 90.00 | 1 | 90.00 |
| 3DR GPS uBlox LEA-6 with Compass | 71.99 | 1 | 71.99 |
| Skywalker 1900 FPV Glider EOP 1900 mm | 81.06 | 1 | 81.06 |
| NTM Prop Drive Series. electric engine | 17.25 | 2 | 34.50 |
| Plane remote control Hobby King 2.4 GHz 6Ch Tx & Rx V2 | 22.10 | 1 | 22.10 |
| Electronic Speed Controller Turnigy AE-80A Brushless ESC | 34.81 | 1 | 34.81 |
| Battery Turnigy nano-tech 8400 mA h 3S 65–130 C LipoPack | 51.44 | 1 | 51.44 |
| LiPo battery FlightPower EON28 LiPo 3S 11.1 V 1800 mA h | 45.69 | 1 | 45.69 |
| Carbon fibre tube | 11.40 | 3 | 34.20 |
| Servo Extension Cables | 1.50 | 4 | 6.00 |
| LiPo battery charger. checker and safe bag | 100.14 | 1 | 100.14 |
| Propeller Mounting + 2 propellers | 4.26 | 3 | 12.78 |
| Hinges | 2.74 | 2 | 5.48 |
| Balsa wood sheet | 2.88 | 2 | 5.76 |
| 12 mm × 1 m aluminium tube | 3.34 | 3 | 10.02 |
| Adhesive fibre tape AXTON 10 m × 50 mm | 4.00 | 3 | 12.00 |
| Adhesive Velcro tape and Plastic tape power xtrem | 10.47 | 1 | 10.47 |
| Raspberry Pi model B+ | 42.91 | 1 | 42.91 |
| Raspberry Pi NoIR Camera and Case | 38.97 | 1 | 38.97 |
| Huawei E173 3G USB Dongle | 22.00 | 1 | 22.00 |
| XBee shield | 44.33 | 1 | 44.33 |
| Arduino UNO | 24.90 | 1 | 24.90 |
| Regulator KA7805A | 0.61 | 2 | 1.22 |
| Total | | | 946.76 |

and the latency to be as low as possible. Therefore, it is necessary to use a lower resolution. After several tests, a resolution of 640 × 320 at 24 fps was chosen because the overall quality was sufficient and most of the Raspberry Pi resources were still available. However, the internet connection is also a limiting factor because the same connection is used to upload the ground sensor's information to the base station, to control the tank discharge system and by the plane to send the telemetry and receive instructions. Thus, the network usage dedicated to the video transmission must be kept as low as possible. This is why the resolution of 240 × 120 pixels at 15 fps was ultimately used. Although they are low, these values still provide an acceptable image quality for achieving the purpose. Furthermore, the video is stored in a flash memory in Full HD quality for later use.

The autopilot obtains information about the movements and situation of the plane. This information is transmitted to the ground station for control of the plane. The autopilot can transmit the telemetry via the 3DR 433 MHz radio system, but it has a range of 1 km. To permit larger distances to the ground station, the autopilot sends the telemetry to the on-board computer, which resends it using the Internet 3G connection to the ground station. The communication between the autopilot and the on-board computer could be using a cable connection, but in order to eliminate cables and to simplify, the 3DR 433 MHz radio system is used.

The plane receives two types of commands: orders to guide its flight and instructions to control the tank discharge system. The first permits manual control of the plane. Usually, the autopilot controls the flight, but, if necessary, the plane can be controlled by a human operator. In addition, if a disease or pest is perceived, the contents of the tank can be released over the infected area. The tank door is controlled using a pin of the GPIO ports of the

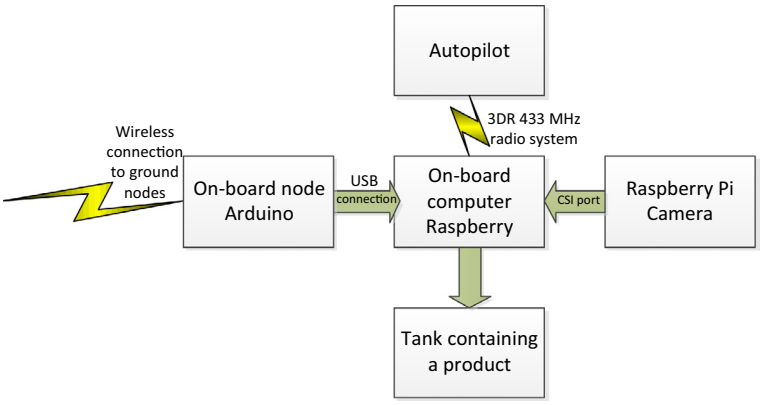


**Fig. 12.** Communication amongst the plane's modules.

Raspberry. The pin drives a servomotor that opens the door of the tank, allowing the substance in the tank to be spread. The operator can open the door and release its contents simply by pressing a button.

Several videos were recorded and can be viewed on the following website:

http://isi.upc.edu/en/research-projects/wsn-with-aerial-mobile-node.

They show several aspects of the developed system: the assembly process; two on-board camera view records, one IR vision and the other normal vision; a ground view of the mobile node flight; and an on-board camera view combined with telemetry information and Google Earth.

Fig. 13 shows the plane and its components before (left) and after (right) assembly.

### 2.4. Stability of the UAV

A simplistic procedure was used to calculate the initial centre of gravity (AIAA, 2007). The method involved the known weights of the internal components and surface area based weight estimations for the external components. The internal known payload, propeller, engine, and pump housing weights were then combined with the external component weights. The distance was calculated from the most forward position of the fuselage to each individual component's centre of mass. The moment for each component was computed, summed, and divided by the total mass.

$$\frac{\sum_i m_i \cdot \overline{X}_i}{\sum_i m_i}$$

When a part of the payload is dropped, the centre of gravity changes. The centre of gravity can also vary with the type of payload carried, for instance, if the payload is a liquid, its location changes during the flight.

In any wing, there is a particular point about which the moments are independent of the angle of attack. This point is defined as the aerodynamic centre for the wing; see Fig. 14. The aerodynamic centre is a useful concept for the study of the aeroplane's stability and control characteristics. In fact, the force and moment system on a wing can be completely specified by the lift and drag acting through the aerodynamic centre, combined with the moment about the aerodynamic centre (Anderson, 1989). The calculation of this point depends on several flow conditions, but, according to (NASA, 2014) for low speed (subsonic) flight and thin airfoils, the position of the aerodynamic centre is considered constant and located at the position 25% of the distance along the chord when the reference point is at the leading edge; see Fig. 14.

The position of the aerodynamic centre relative to the centre of gravity is one of the most important parameters involved in the longitudinal static stability of an aeroplane. A static stability and control study about the three axes is required in order to design a flyable aeroplane. For a neutrally stable wing, the centre of gravity and the centre of lift are co-located. If the wing is disturbed by a gust that increases the angle of attack, the lift will increase but will not result in any restoring torque around the centre of mass. Because there is no rotational torque, this wing will tend to remain where the gust puts it. Thus, it is neutrally stable (Anderson and Eberhardt, 2001). Finally, an unstable wing has its centre of gravity located behind the centre of lift. In that case, if a gust increases the angle of attack, the lift increases, and there is a net rotational torque, which works to increase the angle of attack even further. Any disturbance will be amplified (Anderson and Eberhardt, 2001). This situation is unstable because the wing can reach its stall angle and cause a possible crash.

Thereby, an important parameter that must be checked before the plane is sent into the air is the location of the centre of mass, which must be located closer than to the aerodynamic centre. This calculus has been adjusted in our design for the calculated payload and considering a liquid payload with a volume of 111 ml. This liquid payload is adjusted during the mission To reduce the possibility of a crash. For other liquid values, it is necessary to recalculate the parameters.

## 3. Tests and trials

Several tests were conducted to check the operation of the system. As the system is a first prototype to check its feasibility, the take-off was done, simply, a person launching the plane from the ground. The plane has no wheel for landing, it slides on its belly on the ground until it stops. The plane is robust enough not to suffer any damage.

The objective of the first set of test flights was to check for correct operation of the system consisting of the mobile node, the plane and the other subsystems carried by the plane. Several of the test flights were controlled by an experienced operator using an RC controller, but others were controlled by the on-board autopilot.

In total, nine flights were conducted to test and check for the proper operation of the aircraft and its entire payload. Most of the flights were controlled by the on-board autopilot. Fig. 15 shows one of the programmed waypoint missions with six waypoints to be followed by the autopilot. The mission was to fly a left-handed traffic pattern at 100 m, descend to 75 m when approaching the runway at waypoint 6, then climb again to 100 m to start the pattern again, as in Fig. 15, left. The pattern shown was to be flown indefinitely until manual control was taken by a pilot on the ground. Fig. 15 right shows that the real path flown by the plane does not follow exactly the programmed points of the route. This behaviour was caused by a strong crosswind component that had a major effect in the turns; however, during straight flight, the autopilot was capable of compensating for its effect. The plane flew at the selected altitude for each waypoint.

Fig. 16 shows two laptops receiving the real time video from the on-board IR camera (left laptop) and the telemetry data (right laptop) via the 3G connection.

**Fig. 13.** The mobile node and its components before (left) and after (right) assembly. The total assembly sequence can be seen in a video at http://isi.upc.edu/en/research-projects/wsn-with-aerial-mobile-node.

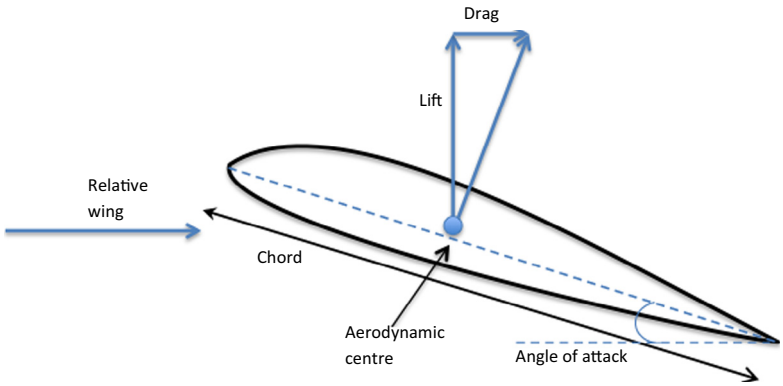


**Fig. 14.** Aerodynamic centre of a wing.

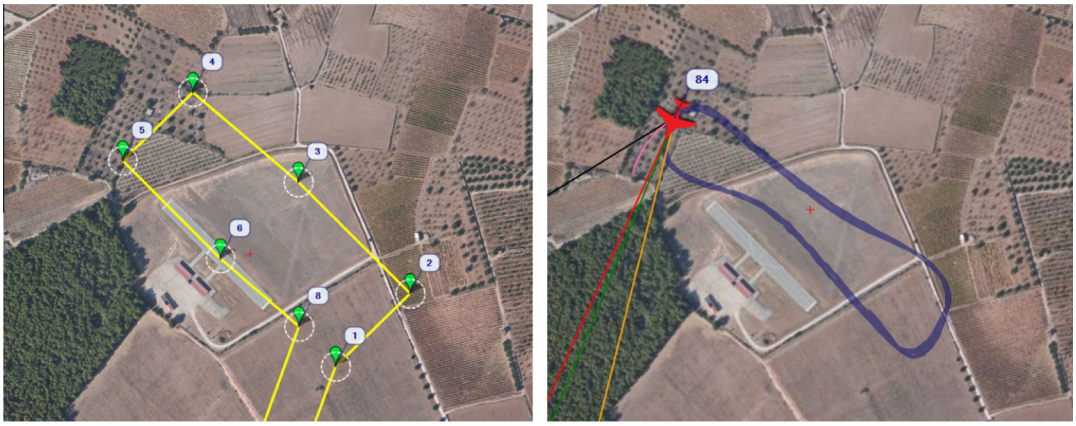


**Fig. 15.** Autopilot-controlled flight. The programmed path for the plane to follow is on the left, and the actual course followed by the plane is on the right.


**Fig. 16.** Ground laptops receiving the real time video and telemetry data from the flying plane.

The plane, carrying the mobile node, flies over the ground nodes scattered throughout the field. The ground nodes are spaced in such a way that they cannot communicate amongst themselves. The mobile node collects the data stored in the ground nodes. When the plane flies over them, it places the on-board mobile node within range of the ground nodes, and the mobile node can connect to the ground nodes and collect their stored data. The sensor data gathering system also fulfilled its task perfectly, uploading the information from the ground sensor.

To obtain a measure of the coverage volume of a node, the ground nodes transmit data continuously. Therefore, the data were only received when the on-board node was within range of the ground nodes. The range was calculated by comparing the time stamps of the data when the data reception began and ended to the GPS position, time stamp and altitude of the telemetry log. This range was approximately 100 m. Fig. 17 shows a ground node, left, its location, centre, and the XBee coverage, right.

The node takes a measurement every 10 min (six times each hour) and stores it in its memory. The mobile node collects the measures once per day.

The size of a measurement is 2 bytes for each parameter, which arises from the 10 bits of the Arduino AD converters, and 3 bytes for its time stamp (hour, minute and second). Two parameters are measured: the temperature and humidity. Therefore, the data


**Fig. 17.** Arduino node, left, its location, centre, and the XBee coverage, right. When the plane flies near the node, it retrieves the data stored in the node.

to retrieve is (2 + 2 + 3) · 24 · 6 = 1008 bytes every day. The Arduino EEPROM memory capacity is 1 KiB (1024 bytes); therefore, it is large enough to store the measured data of an entire day. To avoid data loss when the mobile node cannot collect each day, each node has an SD memory card adaptor to store the measured data.

When the mobile node approaches a ground node, it is awakened by the mobile node. The ground node takes 129 ms to wake up. To send the data from the ground node to the mobile node, the ground node, Arduino, has to send to the wireless transmission module, XBee, and then, the wireless transmission module has to transmit to the mobile node.

The ground node sends the stored data to the XBee module. The module and Arduino are connected using a serial connection at 9600 b/s. Therefore, the data transfer takes 1008 bytes · 8 bits/bytes/9600 b/s = 840 ms. Next, the XBee module transmits the data to the mobile node. The module specification indicates a maximum rate of 250,000 b/s, but our measured transfer rate is slower at 84,000 b/s. The data are transmitted using packets. Each packet has a header, a tail and the payload (data to transmit), Fig. 18. The maximum payload of each frame is 100 bytes, and 1008 B/100 B = 10.1 frames; therefore, 11 frames are necessary to transmit all of the measures. Furthermore, each frame has 16 bytes of header and tail, so the total number of bytes to transmit is 1008 bytes + 11 frames · 16 header = 1184 bytes, and the corresponding transmission time is 1184 B · 8 b/B/84,000 b/s = 113 ms. Fig. 18 shows the structure and transmission time of an XBee frame.

The time necessary to receive the data acquired during 1 day is 129 ms (wake up) + 840 ms (Arduino to XBee) + 113 ms (XBee to mobile node) = 1082 ms.

The maximum velocity of the plane is 35 knots, or 18 m/s. Therefore, the plane moves 19.5 m during the 1082 ms needed for the data reception. As the maximum range for receiving data is approximately 100 m, the maximum height the plane can fly and receive data is approximately 99.5 m. Fig. 19 shows a diagram of the mobile node flying at the maximum permissible height. Usually, the mobile node flies at lower heights, typically 20 m, so it is not necessary to change the flight to receive data.

When the mobile node does not collect the data measured by the ground nodes, these nodes act as data loggers. They save their measurements in their SD memory cards until the mobile node

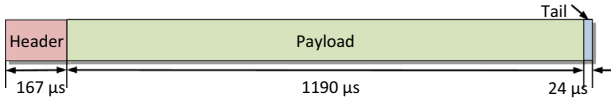


**Fig. 18.** XBee frame transmitted by the ground nodes. It has three fields: the header, 14 bytes; the payload, maximum 100 bytes; and the tail, 2 bytes. The figure shows the transmission time for each field. The total transmission time is 1.38 ms.

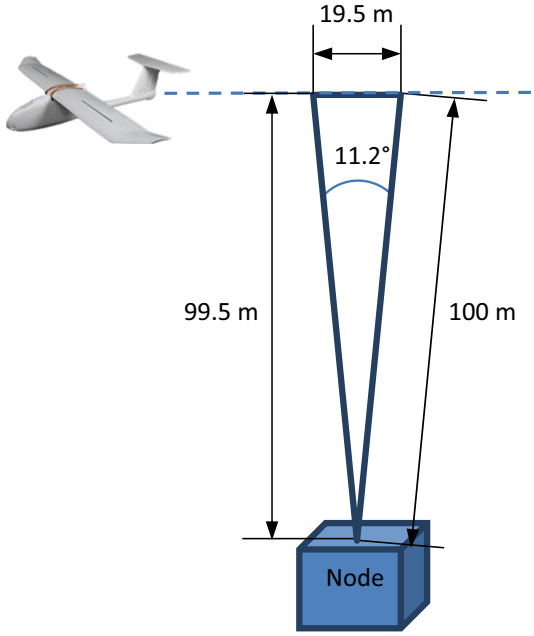


**Fig. 19.** Maximum flight height. The mobile node needs 1082 ms to receive the data, during which it moves 19.5 m. The maximum data reception range is approximately 100 m; therefore, the maximum height is approximately 99.5 m.

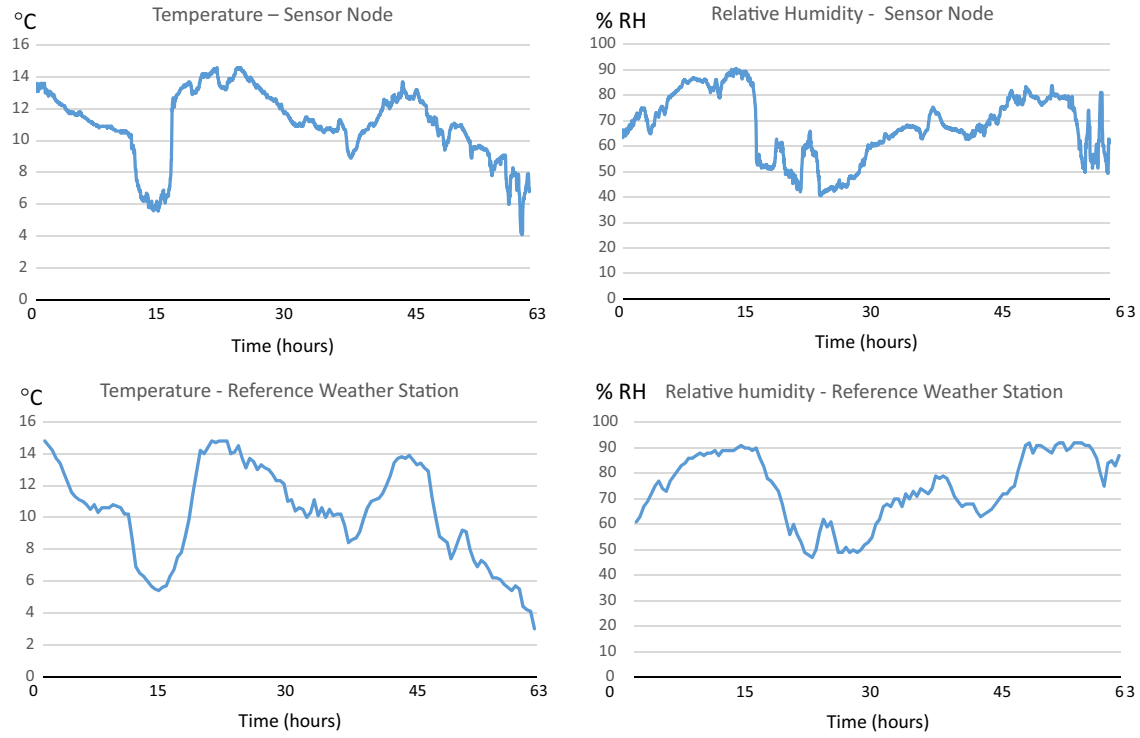


**Fig. 20.** Graphs of the temperature and humidity on February 18, 2015 stored by a sensor node and retrieved by the mobile node.

**Fig. 21.** Scattering sequence. The contents of the on-board tank are disseminated.

flies over again. Fig. 20 shows the temperature and the humidity data for February 18, 2015 stored by a sensor node and retrieved by the mobile node. The ground nodes cannot communicate with each other because they are too far apart.

Because the objective is to design a system for agricultural applications, a small tank has been added to contain products such as insecticides, fertilizers, herbicides, markers or any other contents for fighting a detected disease or pest. Although a fixed-wing UAV is not the most suitable vehicle for spraying, a rotorcraft is better, the plane was equipped with the tank to test its functionality. Fig. 21 shows the sequence of evacuation of the tank. The load capacity essentially depends on the size of the aircraft. Typically, the ratio of the load capacity to the total weight of the aircraft is less than 0.5. One of the initial design requirements is the total weight of the system was 5 kg, including the main aircraft. Because the total weight of the aeroplane is 3 kg, the maximum payload contained in the tank is 2 kg.

To enhance the probability of success when the substance is released, further studies should be performed that account for the flight speed, wind direction and speed when it is released.

Several videos were recorded and can be viewed on this website:http://isi.upc.edu/en/research-projects/wsn-with-aerial-mobile-node.

## 4. Conclusions

A sensor network to be used in large fields has been developed. The sensor nodes are scattered around the field and are too far apart to connect directly each other. A mobile sensor node, or mule, has been designed to collect the data from the static sensor nodes. To transport the mobile sensor node, or mule, an aerial vehicle has been developed.

Several conditions were placed on the design of the sensor network so it would be as flexible as possible: the mobile node must be able to cover distances up to 10 km or to operate in fields of approximately 100 ha; the vehicle must aid in the detection of disease or pests in crops, and if detected, the vehicle must transport substances and launch them when necessary; and the total cost must be low.

The vehicle has several functions to meet these conditions: it transports the mobile node, or mule, to cover large areas; it accesses any location in a short time; it collects data from dispersed ground nodes; to aid the detection of pests or any other problem that affects the plants, the vehicle has a image sensor that sends a video stream; to provide knowledge of the path made by the aerial vehicle, the location of every ground node, and the position of any detected disease or pest, the vehicle sends telemetry

information; and to fight the located pests or to fertilize the plants, the vehicle transports a substance to be scattered.

The aerial vehicle contains several subsystems that enable these functions: the mobile node, an on-board computer, an autopilot, a camera, and a tank.

To check the functionality of the mobile node and the aerial vehicle, several test flights were carried out. The initial flights were made to check the ability of the vehicle to fly. Later, a series of flights was conducted to demonstrate that the system was working properly and that the objectives were achieved.

When the mobile node collects the data stored in a ground node, it needs 129 ms to retrieve the data recorded in 1 day. The usual flight altitude and velocity of the mobile node are 20 m and 18 m/s, respectively, and in this situation, the time the mobile node spends within 100 m of the ground node is 10.9 s. This time is sufficient to retrieve 1814 measures, corresponding to approximately 12.5 days of measurements.

The total cost is approximately $900. This amount is low enough to justify the introduction of our sensor network with a mobile node into any agricultural application with a large field or when global measurements of the field are desired. This network can be applied to supervise plantings of wheat, rice, corn, or any extensive cultivation in which it is difficult to use a traditional sensor network because of large field dimensions and when global measurements of the state of crops and soil are desired.

## Appendix A. Supplementary material

Supplementary data associated with this article can be found, in the online version, at http://dx.doi.org/10.1016/j.compag.2015.09.024.

## References


Abacom ARX-433-ULC. <http://www.abacom-tech.com/%2FUltra-Low-Current-AM-RF-Receiver-Modules-ARX-433-ULC-P93280.aspx> (accessed 16.06.14).

AIAA Undergraduate Team Aircraft Design Competition Concept Design Report. AE 440 November 16, 2007. Agricultural Unmanned Aircraft System Global Agricultural Unmanned Systems.

Anderson Jr., J.D., 1989. Introduction to Flight. McGraw-Hill, pp. 357–409, (Chapter 7).

Anderson, D.F., Eberhardt, S., 2001. Understanding Flight. McGraw-Hill, pp. 15–54, (Chapter 2).

Aqeel-ur-Rehman, Abbasi, A.Z., Islam, N., Shaikh, Z.A., 2014. A review of wireless sensors and networks' applications in agriculture. Comput. Stand. Interfaces 36, 263–270.

Austin, R., 2010. Unmanned Aircraft Systems. UAVs Design, Development and Deployment. John Wiley & Sons Ltd.

Ayalew, G., Ward, S.M., 2000. Development of a prototype infrared reflectance moisture meter for milled peat. Comput. Electron. Agric. 28, 1–14.

Benett, D., 2014. What are the key issues for UAV use in agriculture?, Report from the Southern Cotton Ginners Association Summer Meeting.

Bento, M.D.F., 2008. Unmanned aerial vehicles: an overview. Inside GNSS 3, 54–61.

Chao, H., Cao, Y., Chen, Y., 2007. Autopilots for small fixed-wing unmanned air vehicles: a survey. In: International Conference on Mechatronics and Automation, 2007 (ICMA 2007), 5–8 August 2007, Harbin, China, pp. 3144–3149.

Chiasserini, C.-F., Rao, R.R., 2003. Coexistence mechanisms for interference mitigation in the 2.4-GHz ISM band. IEEE Trans. Wireless Commun. 2 (5), 964–975.

Hassan-Esfahani, L., Torres-Rua, A., Ticlavilca, A.M., Jensen, A., McKe, M., 2014. Topsoil moisture estimation for precision agriculture using unmmaned aerial vehicle multispectral imagery. In: IEEE International Geoscience and Remote Sensing Symposium (IGARSS), 13–18 July 2014, Quebec City, Canada, pp. 3263–3266.

Hea, H., Huanga, M., García, A., Hernández, A., Songa, H., 2007. Prediction of soil macronutrients content using near-infrared spectroscopy. Comput. Electron. Agric. 58, 144–153.

Higuera, J., Polo, J., 2011. Standardization for interoperable autonomous smart sensors in the future energy grid system. In: IEEE 33rd International Telecommunications Energy Conference (INTELEC), 9–13 October 2011, Amsterdam, Holland, pp. 1–9.

Hunt, E.R., Daughtry, C.S.T., Mirsky, S.B., Hively, W.D., 2014. Remote Sensing with simulated unmanned aircraft imagery for precision agriculture applications. IEEE J. Sel. Top. Appl. Earth Observations Remote Sens. 7, 4567–4571.

Lee, Peter, Drones to Take Farming to New Heights. <http://www.taylorvinters.com/news-and-events/news/375-drones-to-take-farming-to-new-heights#.VV9D10-8MXA> (accessed 15.05.14).

Liang, P., Slaughter, D.C., Ortega-Beltran, A., Michailides, T.J., 2015. Detection of fungal infection in almond kernels using near-infrared reflectance spectroscopy. Biosyst. Eng. 137, 64–72.

Liu, G., Ying, Y., 2003. Application of bluetooth technology in greenhouse environment, monitor and control. J. Zhejiang Univ. Agric. Life Sci. 29, 329–334.

López Riquelme, J.A., Soto, F., Suardíaz, J., Sánchez, P., Iborra, A., Vera, J.A., 2009. Wireless sensor networks for precision horticulture in Southern Spain. Comput. Electron. Agric. 68, 25–35.

Measurement Specialities. MS5611-01BA03 Barometric Pressure Sensor. October 2012. <http://www.meas-spec.com/downloads/MS5611-01BA03.pdf> (retrieved 24.05.15).

NASA. Wing Gemoetry Definitions. <http://www.grc.nasa.gov/WWW/k-12/airplane/geom.html> (accessed 11.07.14).

Phillips, W.F., 2010. Mechanics of Flight. John Wiley & Sons, Inc.

Radio Regulations Articles. International Telecommunication Union (ITU).

RPi USB Webcams. <http://elinux.org/RPi_USB_Webcams> (accessed 12.08.14).

Ruiz-Garcia, L., Lunadei, L., Barreiro, P., Robla, J., 2009. A review of wireless sensor technologies and applications in agriculture and food industry: state of the art and current trends. Sensors 9, 4728–4750.

Silverstein, A., 1934. Scale Effect On Clark Y Airfoil Characteristics From N.A.C.A. Full-Scale Wind-Tunnel Tests. National Advisory Committee for Aeronautics. Report No. 502.

ST. LSM303D Ultra-compact high-performance eCompass module. November 2013. <http://www.st.com/web/en/resource/technical/document/datasheet/DM00057547.pdf> (retrieved 24.05.15).

Stafford, J.V., Weaving, G.S., Lowe, J.C., 1989. A portable infra-red moisture meter for agricultural and food materials: Part 1, instrument development. J. Agric. Eng. Res. 43, 45–56.

Suchata, S., Theanjumpolb, P., Karrila, S., 2015. Rapid moisture determination for cup lump natural rubber by nearinfrared spectroscopy. Ind. Crops Prod. 76, 772–780.

Wang, N., Zhang, N., Wang, M., 2006. Wireless sensors in agriculture and food industry – recent development and future perspective. Comput. Electron. Agric. 50, 1–14.

Weyrich, M., Wang, Y., Scharf, M., 2013. Quality assessment of row crop plants by using a machine vision system. In: 39th Annual Conference of the IEEE Industrial Electronics Society, IECON 2013, 10–13 November 2013, Vienna, Austria, pp. 2466–2471.

XBee® 802.15.4. <http://www.digi.com> (accessed 1.08.14).

Yin, Z., Lei, T., Yan, Q., Chen, Z., Dong, Y., 2013. A near-infrared reflectance sensor for soil surface moisture measurement. Comput. Electron. Agric. 99, 101–107.

ZigBee Features. <http://www.zigbee.org/imwp/download.asp?ContentID=11900> (accessed 1.12.14).

ZigBee Specification FAQ. <http://www.zigbee.org/Specifications/ZigBee/FAQ.aspx> (accessed 1.12.14).